Crystal Structure and Magnetic Susceptibility Study of Pyrrolidinium Trichlorocuprate(II)

Mingyi Wei and Roger D. Willett*

Department of Chemistry, Washington State University, Pullman, Washington 99164

Daniel Teske, Kala Subbaraman, and John E. Drumheller*

Department of Physics, Montana State University, Bozeman, Montana 57107

Received January 18, 1996[⊗]

The title compound, $(C_4NH_{10})CuCl_3$, is shown to exist in two phases, the previously reported α phase and a new β phase. DSC studies indicate that the β phase transforms to the α phase at 93 °C. The β phase is stable at the room temperature, with the α phase metastable with respect to the β phase at room temperature. Crystals of the β phase are monoclinic, *C*2/*c*, with $a = 17.327(3)$ Å, $b = 8.360(2)$ Å, $c = 12.005(2)$ Å, and $\beta = 100.92\ (3)°$ with $Z = 8$ for $\rho = 1.883$ *g*/cm^3. The structure contains chains of bibridged $Cu_2Cl_6^{2-}$ dimers running parallel to the *c* direction. This is in contrast to the previously reported α form, which contains uniform chains of face-shared octahedra. The chains in the α phase lie parallel to the unique (monoclinic) axis. Thus, no crystallographic relationships exist between the two compounds and the phase transition must be first order in nature. A unique feature of the phase transition is a decrease in volume as the crystal is heated through the transition. This is a result of the formation of the more compact chains of face-shared octahedra in the high-temperature phase. Magnetic susceptibility studies of the β phase are indicative of competing ferromagnetic and antiferromagnetic coupling, with the onset of long-range order at 7.5 K. The data are interpreted in terms of a ladder chain consisting of ferromagnetic dimers coupled into antiferromagnetic chains through short Cl···Cl contacts.

Introduction

The crystal structure and magnetic properties of the α phase of pyrrolidinium trichlorocuprate(II) have been reported by Nilsen et al.[1] The primitive monoclinic crystal contained chains of face-shared octahedra running parallel to the unique monoclinic *b* axis. The structure is a variant of the 2L form of the hexagonal AMX_3 structure,[2] with an antiferrodistortive sequence of Jahn−Teller distortions superimposed on the nominal octahedral coordination of the Cu(II) ions.[3] Because of our interest in possible dynamic effects in such chains,[4] we began a study of the system. Preliminary investigations revealed the existence of a second crystalline phase (labeled the β phase in this paper) with the same stoichiometry. In this paper we report the crystal structure of the β phase and a study of its thermal and magnetic properties.

Experimental Section

Initial experiments were carried out on a sample provided by Professor K. Emerson of Montana State University. Subsequent studies utilized samples that were prepared at Washington State University, following the general procedure outlined by Nilsen et al.[1] Dissolution of a 1:1 ratio of pyrrolidine and $CuCl_2{\cdot}2H_2O$ in aqueous solutions gave precipitation due to the formation of pyrrolidine-coordinated copper(II) complexes. Concentrated HCl solution was added with stirring until the precipitate disappeared, and then a few more drops of HCl were added to prevent reprecipitation. Crystallizations were carried out from aqueous hydrochloric acid solutions of pyrrolidine and cupric chloride dihydrate whose temperature was varied from room temperature to 90 °C and whose mole ratios were varied over a substantial range. The β form of pyrrolidinium trichlorocuprate(II) was invariably obtained from crystallization at room temperature while the α form could only be crystallized above 90 °C. Crystals used in this study were obtained by evaporation of 1:1 mole ratios of pyrrolidine and $CuCl_2{\cdot}2H_2O$ in aqueous solutions with excess amounts of HCl at 40−60 °C (β phase) or ≥90 °C (α phase).

DSC studies were carried out on both the α and β phases (as identified by X-ray diffraction) with a Perkin-Elmer Delta DSC7 instrument over the temperature range 30−230 °C. Crystalline samples were ground and sealed in the sample pans. Helium gas (flow rate 20 kPa) was used as purge gas. The scan rate of 20 °C/min was used for both calibration and data collection. Each phase showed a major exothermic transition at approximately 200 °C. The β phase exhibited a weak endothermic transition near 93 °C with $\Delta H_{trans} \sim 2.2$ kJ/mol. In the α phase, a very broad endotherm was also observed near 140 °C with $\Delta H_{trans} \sim 1.2$ kJ/mol.

The susceptibility data for both compounds were taken with a Lake Shore 7225 susceptometer/magnetometer at a frequency of 375 Hz and an ac excitation field of 0.4 Oe. The temperature was increased incrementally from 4.2 K. The applied dc field was zero, but the samples were not shielded from Earth's field. The crystals of the α phase were quite small, so that material was measured as a powdered sample. This powdered sample was not stable and over a period of days developed a prominent shoulder at about the temperature where the maximum peak height of β-pyrrolidinium occurs. The β-pyrrolidinium sample was in the form of dark red plates with distinct grooves along one axis, probably indicating that the plates are polycrystalline and fairly well aligned. Susceptibility data were collected with the applied magnetic field aligned parallel to each of the three geometrical axes of a plate. The shape of the peak was essentially the same for all three orientations but was higher for the orientation parallel to the plate and parallel to the grooves. For the orientation parallel to the plate and perpendicular to the grooves, the data were noisier than for the other two orientations. The EPR measurements on crystals of the β phase were made using an X-band spectrometer at a microwave frequency of 9.3 GHz at $T = 15.6$ K. The *g* values obtained from measurements along all the three axes of the crystal were later used to fit the susceptibility data.

[⊗] Abstract published in *Advance ACS Abstracts,* September 1, 1996.

(1) Nilsen, D. M.; Larsen, R. D.; Emerson, K.; Rubenacker, G. V.; Ping, Z.; Drumheller, J. E. *Inorg. Chem.* **1990**, *29*, 2887.
(2) Li, T.; Stucky, G. D.; McPherson, G. L. *Acta Crystallogr.* **1973**, *B29*, 1330. Plumer, L. L.; Hood, K.; Caille, A. *J. Phys. C* **1988**, *21*, 4189.
(3) Willett, R. D.; Bond, M. R.; Haije, W. G.; Soonieus, O. P. M.; Maaskant, W. J. A. *Inorg. Chem.* **1988**, *27*, 614.
(4) Crama, W. J. *Acta Crystallogr.* **1981**, *B37*, 2133.

S0020-1669(96)00057-2 CCC: $12.00

Table 1. Crystal Data and Experimental Details for β-Pyrrolidinium Trichlorocuprate(II)

empirical formula	$(C_4NH_{10})CuCl_3$	fw	242.03
crystal system	monoclinic	temp	23 °C
a, Å	17.327(3)	space group	*C2/c*
b, Å	8.360(2)	λ(Mo Kα)	0.710 73 Å
c, Å	12.005(2)	ρ_{calcd}, g cm^{-3}	1.883
β, deg	100.92(3)	μ(Mo Kα), cm^{-1}	0.341
V, Å^3	1707.5(6)	R,[a] %	5.10
Z	8	R_w,[b] %	6.70

[a] $R = \sum||F_o| - |F_c||/\sum|F_o|$. [b] $R_w = \sum w(|F_o| - |F_c|)^2/\sum|F_o|^2)^{1/2}$.

Table 2. Atomic Coordinates ($\times 10^4$) and Equivalent Isotropic Displacement Coefficients (Å$^2 \times 10^3$) for β-Pyrrolidinium Trichlorocuprate

atom	*x*	*y*	*z*	*U*(eq)[a]
Cu	304(1)	6155(1)	1176(1)	34(1)
Cl(1)	439(1)	3519(2)	620(1)	42(1)
Cl(2)	662(1)	8779(2)	1214(1)	44(1)
Cl(3)	998(1)	5764(2)	2952(1)	41(1)
N(1)	3853(3)	5071(7)	6147(4)	48(2)
C(2)	3100(4)	5750(10)	5550(6)	66(3)
C(3)	2501(5)	4780(16)	5935(10)	120(6)
C(4)	2872(6)	3586(12)	6740(9)	88(4)
C(5)	3713(5)	3471(10)	6601(7)	62(3)

[a] Equivalent isotropic *U* defined as one-third of the trace of the orthogonalized $\mathbf{U}_{ij}$ tensor.

A dark red crystal (0.35 mm × 0.30 mm × 0.15 mm) from the sample provided by Professor Emerson was mounted on a Syntex $P2_1$ diffractometer which had been upgraded to Nicolet P3F specifications and equipped with a graphite monochromator (Mo Kα radiation, λ = 0.710 73 Å). Lattice constants, determined from 25 accurately centered reflections, yielded a *C*-centered monoclinic lattice with a = 17.327(3) Å, b = 8.360(2) Å, c = 12.005(2) Å, β = 100.92(3)°, and V = 1707.5(6) Å^3. This gives ρ_{calc} = 1.883 *g*/cm^3 for Z = 8. These lattice constants did not conform to those previously reported for the compound,[1] so a structure determination was undertaken. Data collection, with a 0.9° ω scan and variable scan speeds from 4.0 to 30°/min, yielded 1325 reflections out to 2θ = 45° (1109 unique, with r_{merge} = 0.027).[5] Empirical absorption corrections, base on ψ scans, were applied (μ = 0.341 cm^{-1}). Crystal data and experimental details are summarized in Table 1. The structure solution proceeded in a straightforward fashion in the centrosymmetric space group *C2/c* utilizing the direct methods program SOLV in the SHELXTL program package on a Data General computer.[6] Final refinement, performed on a VAX 3100 workstation with the SHELXTL-PLUS program package,[7] yielded $R = \sum||F_o| - |F_c||/\sum|F_o| = 0.051$ and $R_w = \sum w(||F_o| - |F_c||)^2/\sum w|F_o|^2 = 0.067$ for all reflections. Hydrogen atoms were included at idealized positions (C−H = N−H = 0.96 Å). Final positional parameters and equivalent isotropic thermal parameters are given in Table 2. Table 3 gives pertinent bond distances and angles.

A crystal from our initial preparation was also mounted on the same diffractometer system. The lattice constants were consistent with those reported by Nilsen et al.[1] (The values we obtained were a = 9.346(1) Å, b = 6.5097(7) Å, c = 14.131(1) Å, β = 102.93(1)°, and V = 837.9 Å^3 with Z = 4 in $P2_1/n$.) Analysis of a data set collected on that crystal confirmed the structure reported by Nilsen.

In addition, crystals of the α and β phases were heated while mounted on the diffractometer and lattice constants monitored as the crystal was heated. The sample of the β phase lost crystallinity between 90 and 100 °C, corresponding to the endotherm observed at 93 °C in the DSC experiment. In contrast, the α phase retained its structure up to 130 °C, at which point it slowly lost crystallinity. Again, this correlates well with the endotherm observed in the DSC study of this phase. The decomposition precluded the pursuit of a crystal structure determination of this additional phase.

Table 3. Bond Lengths (Å) and Bond Angles (deg) for β-Pyrrolidinium Trichlorocuprate[a]

Cu−Cl(1)	2.327(2)	N(1)−C(2)	1.478(9)
Cu−Cl(2)	2.277(2)	N(1)−C(5)	1.481(10)
Cu−Cl(3)	2.264(2)	C(2)−C(3)	1.460(14)
Cu−Cl(1A)	2.30(2)	C(3)−C(4)	1.452(15)
Cu−Cl(3B)	2.681(2)	C(4)−C(5)	1.501(13)

Cl(1)−Cu−Cl(2)	151.2(1)	Cl(1A)−Cu−Cl(3B)	91.0(1)
Cl(1)−Cu−Cl(3)	94.0(1)	Cu−Cl(1)−Cu(A)	95.0(1)
Cl(2)−Cu−Cl(3)	91.5(1)	Cu−Cl(3)−Cu(B)	90.8(1)
Cl(1)−Cu−Cl(1A)	85.0(1)	C(2)−N(1)−C(5)	109.5(5)
Cl(2)−Cu−Cl(1A)	90.4(1)	N(1)−C(2)−C(3)	104.4(7)
Cl(3)−Cu−Cl(1A)	177.8(1)	C(2)−C(3)−C(4)	109.9(8)
Cl(1)−Cu−Cl(3B)	97.7(1)	C(3)−C(4)−C(5)	106.7(9)
Cl(2)−Cu−Cl(3B)	110.8(1)	N(1)−C(5)−C(4)	102.3(6)
Cl(3)−Cu−Cl(3B)	87.2(1)		

[a] A denotes atom coordinates related by $-x, -y, -z$. B denotes atom coordinates related by $-x, y, {}^1/_2 - z$.

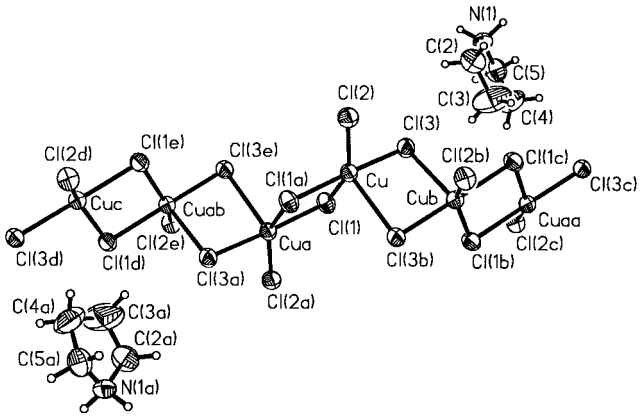

Figure 1. Illustration of the dimer chain in the β phase, with thermal ellipsoids included at the 50% probability level.

Structure Description

The β phase structure contains centrosymmetric bibridged $Cu_2Cl_6^{2-}$ anions that are linked together through semicoordinate bonds to yield infinite, alternating bibridged chains that run parallel to *c*. The chain structure is illustrated in Figure 1. In this manner, each Cu(II) ion attains a commonly observed folded 4+1 coordination[8] with $(Cu-Cl)_{av}$ = 2.294(3) Å in the basal plane and with the semicoordinate (axial) bond length equal to 2.681(2) Å. The basal plane shows a pronounced folding with a smaller *trans* angle of Cl(1)−Cu−Cl(2) = 151.2(1)°. The chain structure is similar to that in $[(CH_3)_2NH_2]CuCl_3$[9] and corresponds to the stacking diagram **I**, where adjacent dimers are related by the *c* glide symmetry elements. This arrangement is labeled a $2({}^1/_2, {}^3/_2, 90°)$ stacking pattern in the Geiser notation.[10]

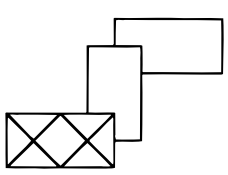

I

(5) Campana, C. F.; Shepard, D. F.; Litchman, W. M. *Inorg. Chem.* **1981**, *20*, 4039.
(6) Sheldrick, G. M. *SHELXTL User's Manual*, Version 5.1; Nicolet Instrument Corp.: Madison, WI, 1986.
(7) Sheldrick, G. M. *SHELXTL-PLUS*; Siemens Analytical Instruments, Inc: Madison, WI, 1990.
(8) Blanchette, J.; Willett R. D. *Inorg. Chem.* **1988**, *27*, 843.
(9) Willett, R. D. *J. Chem. Phys.* **1965**, *44*, 39.
(10) Geiser, U.; Willett, R. D.; Lindbeck, M.; Emerson, K. *J. Am. Chem. Soc.* **1986**, *108*, 1173. Bond, M. R.; Willett, R. D. *Inorg. Chem.* **1989**, *28*, 3267. Willett, R. D.; Bond, M. R.; Pon, G. *Inorg. Chem.* **1990**, *29*, 4160.

Table 4. Two-Halide Contacts for the Pyrrolidinium Trichlorocuprates[a]

phase	atoms	dist, Å	atoms	angle, deg
α	Cl(1)−Cl(2a)	4.143	Cu(1)−Cl(1)−Cl(2a)	139.9
			Cu(2a)−Cl(2a)−Cl(1)	138.2
β	Cl(2b)−Cl(2c)	3.924	Cu(b)−Cl(2b)−Cl(2c)	111.6
	Cl(1)−Cl(2c)	4.033	Cu(b)−Cl(1)−Cl(2c)	107.4
			Cu−Cl(1)−Cl(2c)	153.1
			Cu(c)−Cl(2c)−Cl(1)	157.9

[a] a denotes atom coordinates transformed by $^1/_2 - x$, $-^1/_2 + y$, $^1/_2 - z$. b denotes atom coordinates transformed by $-x$, $1 - y$, $-z$. c denotes atom coordinates transformed by $-x$, $2 - y$, $-z$.

In the *β* form, the $-NH_2$ moiety of each pyrrolidinium cation forms a pair of bifurcated hydrogen bonds to the chloride ions (see Table 4). One type of bifurcated N−H···Cl hydrogen bond links dimers within chains (N−Cl(2) = 3.265 Å and N−Cl(1) = 3.0 Å). The second type bridges adjacent chains (N−Cl(1) = 3.0 Å and N−Cl(2) = 3.288 Å). It is the latter interaction that forces the short interchain Cl···Cl contacts (*vide infra*). For comparison, in the α form, the pyrrolidinium cations are hydrogen-bonded to a pair of chloride ions, one in each of two adjacent chains (N−Cl(2) = 3.297 Å, N−Cl(1) = 3.299 Å). In the *β* phase, the cations are nonplanar, with the N atom lying 0.32 Å out of the plane of the four carbon atoms. However, C(3) shows a large amplitude of thermal motion perpendicular to the plane (0.45 Å), with C(2) showing a somewhat lesser motion (0.28 Å). All bonds are shorter than expected for a rigid molecule. In contrast, in the α phase, the pyrrolidinium ring is nearly planar. The mean deviation from the plane is only 0.014 Å.

In both phases, the $C_4H_8N_2^+$ cation can be fitted by a rigid-body model utilizing the TLS analysis given in the SHELXTL-PLUS program. However, a good least-squares fit of the parameters of the model to the anisotropic displacement parameters of the cation does not necessarily mean that the cation is rigid. In both phases, the C atoms opposite the N atom of the ring have large displacement amplitudes perpendicular to the plane of the ring. Thus both phases show evidence of disorder of the organic cations. However the extent of disorder is larger in the α phase, as evidenced by larger atomic displacement parameters and more nearly planar average structure for the cation.

For interpretation of the magnetic measurements, examination of interspecies contacts is of importance. Figure 2a,b illustrates the observed Cl···Cl contacts in the α and *β* phases, respectively. In the α phase, the shortest interchain Cl···Cl distance is 4.143 Å between Cl(2) and Cl(1). This couples the tribridged $(CuCl_3)_n^{n-}$ chains into a rectangular array that lies parallel to the {101} planes. In the *β* phase, the shortest interchain Cl···Cl distances are 3.924 Å between pairs of Cl(2) atoms and 4.033 Å between Cl(1) and Cl(2) atoms. This couples the chains together into a more complex two-dimensional array, which now lies parallel to the {100} planes.

The Phase Transition

Figure 3 shows the packing of the cations and anionic chains in the two phases (top, α phase; bottom, *β* phase). Examination of the two diagrams in Figure 3 clearly shows the very close structural relationship that exists between the two phases. The general arrangements of cations and anionic chains are nearly unchanged in the two structures. In particular, each anionic chain is surrounded by six stacks of the organic cation, with the chains arrayed in a pseudohexagonal arrangement. The most obvious difference is the reorientation of the pyrrolidinium rings. In the α phase, the normal to the mean plane lies nearly parallel to the anionic chains. In contrast, in the *β* phase, the normal to the plane of the organic ring lies perpendicular to the chains. A second, more crucial difference is associated with the change in symmetry elements that occurs in the phase transition. In the α phase, the uniform chain runs parallel to the unique (*b*) monoclinic axis. However, in the *β* phase, the dimer chains run perpendicular to the unique monoclinic axis. The transformation between the two polymorphs thus involves the creation of new symmetry elements as well as the destruction of existing elements. The phase transition is then clearly first order in nature, consistent with the observed loss of crystallinity upon heating the *β* phase through the transition at 93 °C.

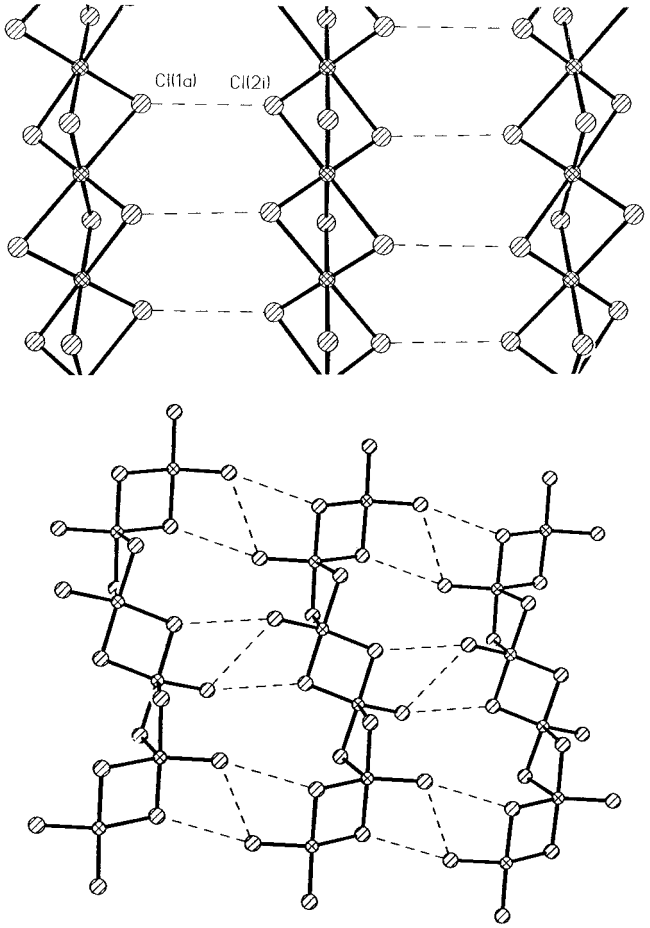

Figure 2. Illustration of interchain contacts. (a) Top: the α phase. The *b* axis is vertical, and the *a* axis is horizontal. (b) Bottom: *β* phase. The *c* axis is vertical, and the *b* axis is horizontal.

An unusual feature of the phase transition is that the molar volume decreases upon going from the low- to high-temperature phase. The molar volume in the low-temperature phase, 213.4 Å^3 decreases by 4.0 Å^3 to 209.4 Å^3 in the high-temperature phase. This must be associated with the more compact nature of the tribridged chain when compared to the more open structure of the dimer chain. This can be seen by inspection of Figure 3. In the tribridged chain, the Cu(II) ions are coordinately saturated, while the 4+1 geometry in the dimer chain has one coordination site unoccupied. The driving force of the transition must be the entropy increase associated with the increased disorder of the cations. This is able to override the more normal tendency of structures to become more open at higher temperatures.

Magnetic Behavior

In order to confirm that the original susceptibility study was carried out on the correct (α) phase, measurements were made on samples of both phases. Figure 4 shows the low-field ac magnetic susceptibility of a powder sample of the α phase. The

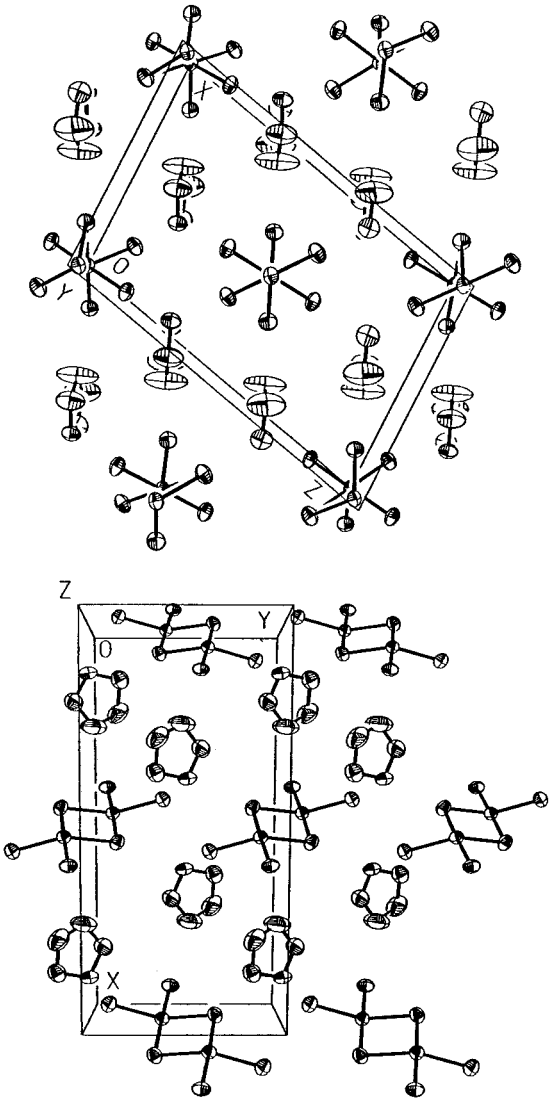

Figure 3. Illustration of the packing of the cations and chains. (a) Top: α phase, as viewed parallel to the *b* axis. (b) Bottom: β phase, as viewed parallel to the *c* axis.

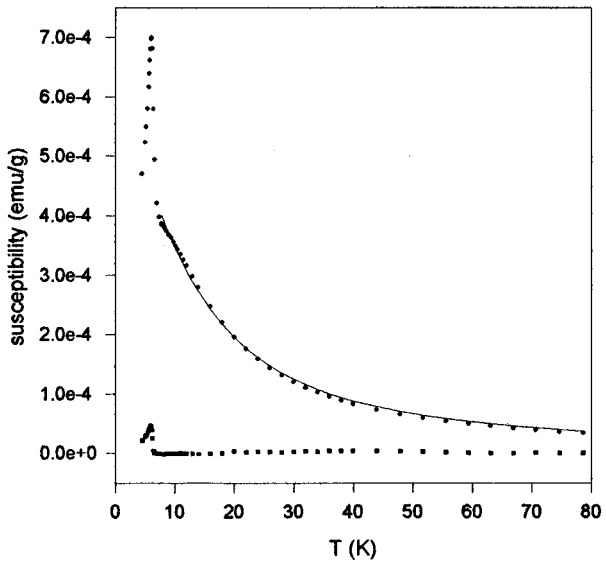

Figure 4. Plot of χ'_M vs *T* for the α phase. The solid line is the best fit to the mean field corrected 1D Heisenberg model with $J/k = 62$ K and $zJ' = -1.2$ K.

plot of $\chi'_M T$ vs *T* (not shown) shows that the $\chi'_M T$ value initially increase as *T* decreases, indicating dominant FM interaction. However, below $T \sim 25$ K, the $\chi'_M T$ product begins to drop.

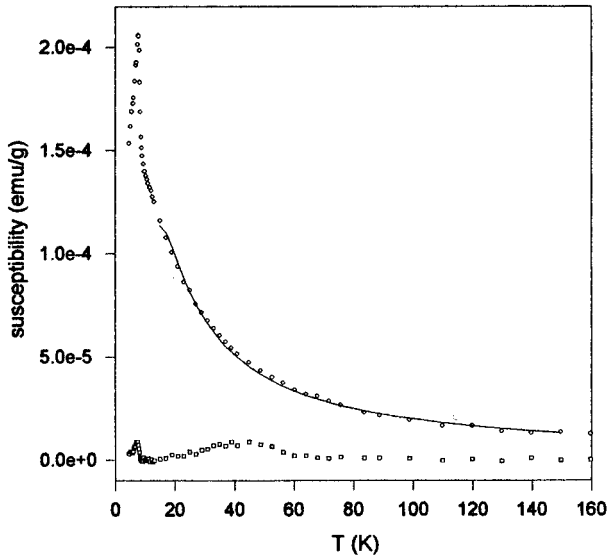

Figure 5. Plot of χ'_M vs *T* for the β phase with H_0 perpendicular to the *bc* plane. The solid line is the best fit to a ladder model with $J/k = 12.3(4)$ K and $J'/k = -1.80(7)$ K with $g = 2.218(7)$.

This provides evidence of the presence of weaker AFM coupling in the system. The onset of long-range order at low temperature is evident from the sharp maximum in χ'_M as well as the step in χ''_M. The former is likely due to the presence of spin canting, while the latter arises from the absorption of energy due to domain wall movement just below T_c. The high-field static susceptibility previously reported is in agreement with the χ'_M data, except that the 3d ordering peak was suppressed in the high-field measurements. The Néel temperature, T_N, is estimated at 6.10 K from the maximum in χ'_M and from the inflection in χ''_M. The high-temperature data were fit to a high-temperature series expansion for a spin $^1/_2$ Heisenberg FM chain with ferromagnetic coupling (J)[11] modified with a mean field correction (J') for AFM interchain interactions, with *g* fixed at 2.191. The analysis of the data between 8 and 80 K yields $J/k = 60$ K and $zJ'/k = -1.6$ K. The value of *J* is extremely sensitive to the *g* value assumed, because of the strong coupling between *g* and *J*. These values of *J* and *J'* are in good agreement with the previous results ($J/k = 56$ K and $zJ'/k = -1.2$ K for $g = 2.191$). On the basis of the structural characteristics, the FM coupling is associated with the tribridged chains while the AFM coupling is associated with the Cl···Cl interchain contacts that are shown in Figure 3a.

Susceptibility measurements on crystals of the β phase along all three crystal axes exhibited very similar behavior. Figure 5 shows the plot of χ'_M and χ''_M vs *T* for H_0 applied perpendicular to the *ac* plane. All measurements showed sharp maxima in χ'_M at 7.5 K, with an associated step in χ''_M. The value of χ'_M(max) was slightly higher for H_0 parallel to *c* (0.060 emu/mol) than in the other two orientations (approximately 0.050 emu/mol). In the temperature range 10−40 K, the value of χ'_M was slightly higher for H_0 perpendicular to the *bc* plane than for H_0 in the plane. The plot of $\chi'_M T$ vs *T* for H_0 perpendicular to the *bc* plane (Figure 6) shows a broad maximum in the range 30−60 K. The initial increase in $\chi'_M T$ as *T* decreases indicates that dominant FM interactions are present. This is also evident for the $1/\chi'_M$ vs *T* plot (not shown), where the high temperature extrapolates to a positive intercept with the temperature axis. The decrease in the value of $\chi'_M T$ in the range 10−30 K indicates the additional presence of weaker AFM coupling in the system.

(11) Baker, G. A., Jr.; Rushbrooke, G. S.; Gilbert, H. E. *Phys. Rev.* **1964**, *135*, 11272.

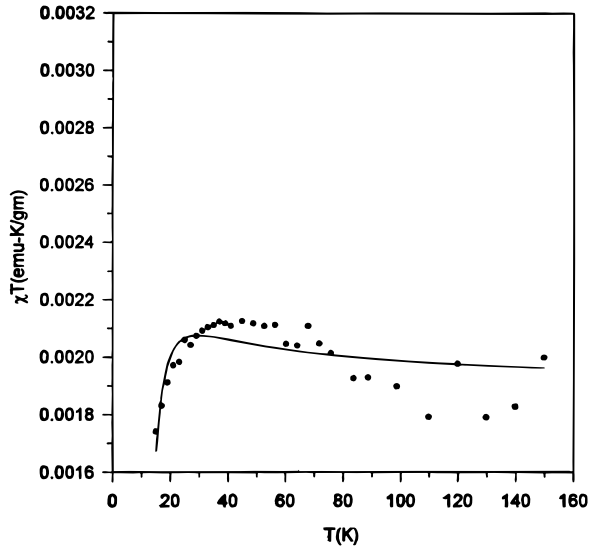

Figure 6. Plot of $\chi'_M T$ vs T for the β phase with H_0 perpendicular to the *bc* plane. The solid line is the best fit to a ladder model with $J/k = 12.3(4)$ K and $J'/k = -1.80(7)$ K with $g = 2.218(7)$.

Additional information can also be deduced. The sharp peak in χ'_M at 7.5 K is again indicative of the presence of spin canting. This sharp peak masks the normal maximum associated with the presence of antiferromagnetic spin correlations, the onset of which can just be observed at the high-temperature side of the maximum. The Néel temperature can thus be taken as 7.5 K. The anomaly in χ''_M at 7.5 K is again likely due to domain wall movement as long-range order sets in.

To proceed further with the analysis, it is necessary to appeal to the known magneto−structural correlations in copper(II) halide systems. Within the copper chloride chains, J denotes the coupling between Cu atoms in the dimeric units and αJ denotes the coupling between dimers. The possible interchain couplings are denoted by J' (the Cl(1)···Cl(2) contacts) and J'' (the Cl(2)···Cl(2) contacts). Three limiting cases can be identified: (i) J, $\alpha J \gg J'$, J'' (defining an alternating chain system); (ii) J, $J' \gg \alpha J$, J'' (defining a ladder chain with J associated with the rungs and J' with the rails); (iii) J, $J'' \gg \alpha J$, J' (defining an alternating chain system also).

It is known that the sign of exchange coupling in $Cu_2Cl_6^{2-}$ dimers depends on the magnitude of the bridging Cu−Cl−Cu angle and the deviation of the Cu(II) coordination geometry from planarity.[12] With a relatively small bridging angle of 95.0(1)° and the bifold angle of 28.9°, ferromagnetic coupling ($J > 0$) within the dimer is anticipated with a J/k value of 10−20 K. The presence of ferromagnetic coupling within the dimer is also required by the presence of spin canting, since the two magnetic centers in a dimer are related by a center of inversion. While the exchange coupling, αJ, between dimers has a variable, not easily parametrized, magnitude, it generally is weak.[13] Thus $|\alpha|$ can be assumed to be $\ll 1$. In contrast, short Cl···Cl contacts between magnetic centers can lead to quite strong antiferromagnetic exchange in favorable circumstances.[14] Thus J' and J'' may be associated with the observed antiferromagnetic behavior at low temperature. For the J' (Cl(1)···Cl(2)) pathway, the Cu−Cl···Cl angles are nearly linear. In contrast, the bond angles are close to 90° for the J'' (Cl(2)···Cl(2)) pathways. The magnetic electrons lie primarily in $d_{x^2-y^2}$ type orbitals on the metals and are further delocalized into σ type p orbitals on the halides. The linear arrangement will lead to much more effective overlap of the wave funtions and thus to much stronger antiferromagnetic exchange. This implies that the J' interaction is presumably the dominant antiferromagnetic exchange pathway. This defines a ladder exchange network with ferromagnetic intradimer exchange (J) for the rungs and antiferromagnetic two-halide contacts (J') for the rails. The data for the orientation with H_0 perpendicular to the *bc* plane were fit to a high-temperature series expansion[15] for a ladder system, to yield $J/k = 12.3(4)$ K and $J'/k = -1.80(7)$ K with $g = 2.218(7)$.

Discussion

It is instructive to compare this system with the very similar phase sequence found in $[(CH_3)_2CHNH_3]CuCl_3$.[16] The latter compound contains a dimer chain structure at room temperature (triclinic, $a = 11.692$ Å, $b = 7.804$ Å, $c = 6.106$ Å, $\alpha = 79.00°$, $\beta = 122.60°$, $\gamma = 116.47°$, and $V = 419.3$ Å^3). It undergoes a first order phase transition at 51 °C to a uniform chain of face-shared octahedra (orthorhombic, $a = 14.589$ Å, $b = 7.296$ Å, $c = 6.365(3)$ Å, and $V = 816.8$ Å^3). Thus there is a somewhat larger decrease in molar volume in this compound, with $\Delta V_M = -5.4$ Å^3. The value of ΔH_{trans} is also somewhat larger at 5.8 kJ/mol, with $\Delta S_{trans} = 18$ J/(mol deg). The stacking of dimers in the low-temperature phase is now a $2(^1/_2, ^3/_2)$ pattern, as illustrated in **II**, and is different from that observed for the

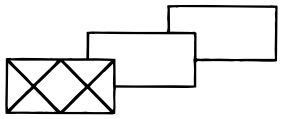

II

β phase of $(C_4NH_{10})CuCl_3$. Examination of packing diagrams in $[(CH_3)_2CHNH_3]CuCl_3$ revealed that the packings of the chains and cations were very similar in the two phases, and indeed, it was possible to transform the low-temperature phase into the high-temperature phase without losing crystallinity. This was despite the fact that the low-temperature space group was not a maximal subgroup of the high-temperature phase. The organic cation was found to be ordered in the low-temperature phase but disordered in the high-temperature phase.

This study emphasizes the crucial role that hydrogen bonding plays in determining the details of structures observed for organoammonium salts of copper(II) halide salts.[17] For the $ACuX_3$ systems, hydrogen-bonding cations stabilized chain type structures based on edge-sharing of CuX_5 square pyramids.[18] In these structures, the existence of nonbridging halide ions is generally associated with multiple N−H···Cl hydrogen bonds to those halide ions. In contrast, the face-shared octahedral structure is obtained with Me_4N^+, while larger R_4N^+ cations yield structures with isolated $Cu_2X_6^{2-}$ dimers.

Acknowledgment. The support of NSF Grants CHE-9113409 (R.D.W.) and DMR-9310967 (J.E.D.) is gratefully acknowledged.

Supporting Information Available: Tables S1−S3, giving crystal data and details of the structure determination, anisotropic thermal parameters, and hydrogen atom coordinates (4 pages). Ordering information is given on any current masthead page.

IC960057F

(12) Scott, B.; Willett, R. D. *J. Appl. Phys.* **1987**, *61*, 3289. O'Brien, S.; Gaura, R. M.; Landee, C. P.; Ramakrishna, B. L.; Willett, R. D. *Inorg. Chim. Acta* **1987**, *141*, 83.
(13) Hatfield, W. E. In *Magneto-Structural Correlations in Exchange Coupled Systems*; Willett, R. D., Gatteschi, D., Kahn, O, Eds.; D. Reidel Publishing Co: Dordrecht, The Netherlands, 1985; p 555.
(14) Halvorson, K.; Willett, R. D. *Acta Crystallogr*. **1988**, *C44*, 2071.
(15) Ping, Z.; Drumheller, J. E.; Rubernacker, J.; Halvorson, K.; Willett, R. D. *J. Appl. Phys.* **1991**, *69*, 5804.
(16) Roberts, S. A.; Bloomquist, D. R.; Willett, R. D.; Dodgen, H. W. *J. Am. Chem. Soc*. **1981**, *103*, 2603.
(17) Willett, R. D.; Geiser, U. *Acta Chim. Crot.* **1984**, *57*, 751,
(18) Geiser, U.; Gaura, R. M.; Willett, R. D.; West, D. X. *Inorg. Chem.* **1986**, *25*, 4203.